Accepted Manuscript

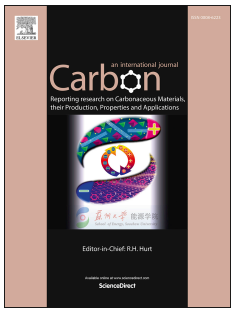

Helically coiled carbon nanotubes as supercapacitor electrodes

Anthony Childress, Kevin Ferri, Apparao M. Rao

PII: S0008-6223(18)30798-X

DOI: 10.1016/j.carbon.2018.08.064

Reference: CARBON 13419

To appear in: *Carbon*

Received Date: 14 June 2018

Revised Date: 24 August 2018

Accepted Date: 30 August 2018

Please cite this article as: A. Childress, K. Ferri, A.M. Rao, Helically coiled carbon nanotubes as supercapacitor electrodes, *Carbon* (2018), doi: 10.1016/j.carbon.2018.08.064.

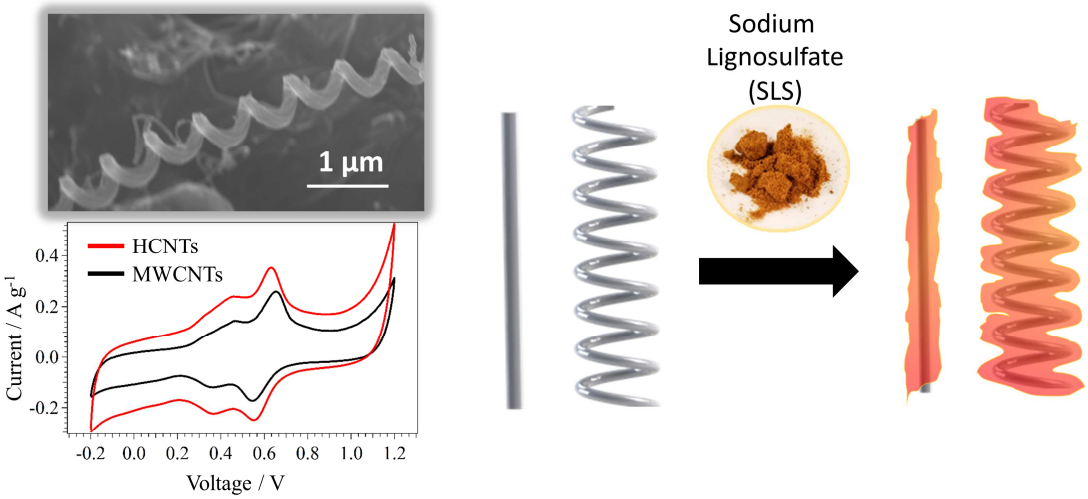

Helically Coiled Carbon Nanotubes as Supercapacitor Electrodes

Anthony Childress[1], Kevin Ferri[2], Apparao M. Rao[1*]

1. Department of Physics and Astronomy and Clemson Nanomaterials Institute, Clemson University, Clemson, SC 29634

2. Department of Materials Science and Engineering, Pennsylvania State University, University Park, PA 16802

Abstract: Despite their low specific surface area (<500 m^2 g^{-1}) relative to that of activated carbon (1500-2000 m^2 g^{-1}), carbon nanotubes are attractive as effective electrode materials for supercapacitors. Electrodes comprised of arrays of helically coiled carbon nanotubes (HCNTs) and multi-wall carbon nanotubes (MWCNTs) were prepared and evaluated as novel electrode materials for electric double layer capacitors (EDLCs). While both types of electrodes exhibited a linear dependence on array height and a diffusion limited behavior below the 1 V s^{-1} scan rate, the electrodes comprised of HCNT arrays exhibited a better performance. Freestanding HCNT and MWCNT buckypapers were also prepared and used as electrodes, and the former showed a higher energy density relative to the latter with no loss in its power density and capacity fade. Collectively, this study concludes that HCNTs are well suited as binder-free electrodes that can be augmented with electroactive polymers for improved EDLC performance.

1. Introduction

Carbon nanotubes (CNTs) have long been considered for use in energy storage materials. In particular, their use in supercapacitors or electric double-layer capacitors (EDLCs) has been a topic of great interest for over a decade. Although CNTs typically have a specific surface area of less than 500 m^2 g^{-1},[1] which is relatively low compared to the ~2000 m^2 g^{-1} of activated carbon,

*Corresponding author. Tel: 864 656-6759 E-mail: arao@clemson.edu

their electrical conductivity, chemical stability, and mechanical robustness lead to high capacitance and power densities when they are integrated into EDLCs. This is mainly due to the mesoporous structure of CNT electrodes which allows for better electrolyte flow and ion access.[2,3] Current densities as high as 100 A g^{-1} have been demonstrated using CNT electrodes with little loss of performance.[4] Moreover, CNT electrodes require less amounts of binders and conductive additives compared to activated carbon based electrodes, and vertically aligned carbon nanotube arrays (VACNTs) with high areal density can be grown directly on current collectors, which reduces contact resistance and mitigates the need for binders. Electrodes made in this manner can possess gravimetric capacitance in excess of 100 F g^{-1}. [5–13] Emphasis has also been placed on growing VACNTs in a continuous scalable fashion such that the current collectors can be wound directly into a useable product.[14–17]

In most previous studies, linear CNTs (multi-wall carbon nanotubes; MWCNTs) were used in the EDLCs. In-depth studies focused on the use of helically coiled carbon nanotubes (HCNTs) which were first synthesized soon after the initial discovery of MWCNTs [18] have not been reported to date. An HCNT is a MWCNT with a helical shape, and they can be grown in vertically aligned arrays (VHCNTs) wherein the coils of adjacent HCNTs are nested together and aligned in pitch.[19] VHCNTs grown directly on current collectors offer a greater surface area per tube for a given array height compared to linear VACNTs, thus increasing the active surface area per unit area of the current collector. In addition, VHCNTs are known to possess superior mechanical properties compared to those of their linear counterparts – they are highly compressible and thus mitigate impact force, leading to their use as impact absorption media for sensitive electronics and additives in epoxy based composites.[20–23] However, little research has focused on using HCNTs as an active material for EDLCs. Zeng *et al.* used iron tartrate as a

catalyst to grow helical carbon nanocoils that were made into electrodes using a standard slurry recipe, yielding capacitance values of ~100 F g^{-1}.[24] In general, coils such as these are thicker in diameter compared to HCNTs and lack the regular graphitic lattice structure. Reddy *et al.* reported a capacitance of ~105 F g^{-1} for symmetric capacitors made from helical carbon nanocoils prepared on Si substrates. [25] Rakhi *et al.* integrated helical carbon nanocoils into a conductive polymer slurry, and coated a carbon cloth.[26] Beyond these reports, a comprehensive investigation into the potential advantages of using HCNTs in EDLCs has not yet been undertaken. Here, we evaluate the electrochemical performance of HCNTs in two types of electrodes – as VHCNTs, and as freestanding polymer-augmented HCNT buckypapers (BPs) which incorporate lignin as the electroactive polymer. Their performance is compared directly to analogous electrodes made with linear MWCNTs. We also evaluate the electrochemical performance of CNT arrays after argon plasma treatment. This investigation is motivated by previous work that showed improved capacitance in few-layer graphene subjected to plasma treatment.[27]

Several theoretical models have been proposed to explain the growth mechanism of HCNTs.[19,28,29] During CNT growth via the chemical vapor deposition method, the use of catalyst particles that contain other elements in addition to iron alters the surface interactions between the metal catalyst particles and the hydrocarbon precursors that break down to form CNTs. The mixed metal catalyst causes the carbon to be extruded at different rates on different sites of the particle surface, producing stresses in the hexagonal lattice of the CNTs, which leads to the helical shape. It has also been proposed that the helical growth is due to rotation of the catalyst particles. As the carbon is extruded at different rates from the different metal faces of the particle, stress can be generated perpendicular to the growth direction, resulting in torsion on the catalyst particle and subsequent rotation.[30] The shape of the particle can also play a role in the growth process.[31]

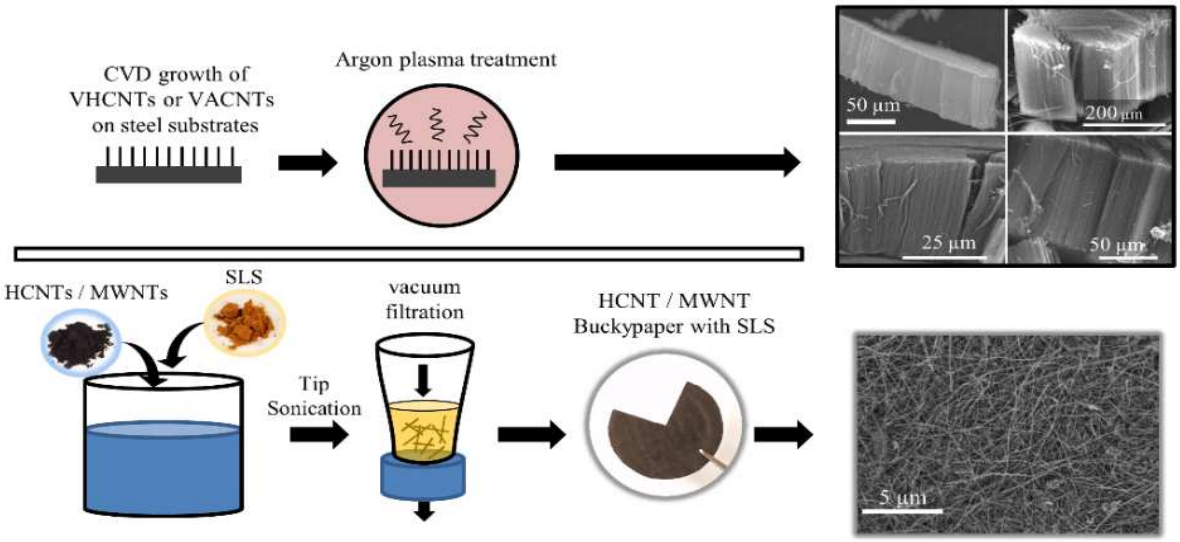

Figure 1. Fabrication procedure for the different electrodes used in this study. The top row outlines the procedure for growing VACNT and VHCNT arrays on steel substrates, and the bottom row shows the steps involved for fabricating the BPs, where sodium lignosulfate (SLS) is the surfactant. For the arrays grown on steel, 1 M $TEABF_4$ in acetonitrile is used as the electrolyte whereas 1 M HNO_3 is used as the electrolyte for the BPs.

Typically, an HCNT is in a higher energy state relative to a linear CNT due to its inherent compressive and tensile stresses, and is therefore more susceptible to chemical modification of its surface. Moreover, defects in the form of pentagons and heptagons within the hexagonal lattice of CNTs are known to lead to local differences of charge density.[32–34] For this reason, we hypothesized that HCNTs should be more susceptible to defects when exposed to an Ar plasma, which can then be measured as a change in the capacitance. This encompasses the first part of this study wherein the electrochemical performances of VANCT and VHCNT arrays grown on conducting substrates are compared before and after their exposure to an Ar plasma (Fig. 1).

For the second part of the study, an electroactive polymer is incorporated into free standing BPs. BPs are tightly packed networks of randomly oriented CNTs, and their structural properties

largely depend on the quality of nanotubes used during their preparation.[35] Typically, they are prepared by dispersing CNTs in water through the use of surfactants such as sodium dodecyl sulfate (SDS). The aqueous CNT dispersion is vacuum filtered to obtain a network of randomly oriented CNTs, which is peeled from the filter paper and air dried to yield a BP. The fabrication steps for the BPs are shown in the lower half of Fig. 1. They are chemically robust, flexible, conductive, and mesoporous scaffolds, which makes them ideal for use with electroactive polymers and as EDLC electrodes. Previously, polymers such as polyurethane,[36] polycarbonate,[37] epoxy resins,[35] and polyethyl ethyl ketone[38] among others have been impregnated into BPs. In the present work, BPs constructed from MWCNTs and HCNTs are fabricated with sodium lignosulfate (SLS) and their electrochemical performances are compared. The electroactive SLS polymer is capable of undergoing a reversible redox reaction, which can increase the energy density of the BP EDLCs. Such CNT-polymer composite electrodes can be prepared by either including the polymer in the CNT dispersion or by direct polymerization on the surface of the BP.[26] With an additional step of soaking the BPs in an SLS solution, the polymer can further infiltrate the spaces between the CNTs, resulting in a greater mass loading of SLS than would be possible in the initial fabrication process of the CNT-SLS BP electrode.

Lignin is a naturally occurring polymer which is separated from cellulose and discarded during the production of paper products, making it a highly abundant and low-cost additive.[39] Past research has shown SLS to be amenable for use with carbon nanomaterials, possibly due to the favorable π-π interaction between the aromatic quinone groups and the hexagonal carbon lattice.[40–42] The quinone groups undergo a redox reaction in acidic media at ~0.5 V with respect to Ag/AgCl. Since the backbone of the lignin polymer is not highly conductive, the

charge transfer is localized at the quinone site, which leads to sharper redox peaks than would be found for conductive electroactive polymers.

2. Experimental

2.1 Synthesis of vertically aligned carbon nanotube arrays

As the growth temperature of HCNTs (~750°C) is well above the melting point of aluminum, steel substrates were used for synthesis of both VHCNTs and VACNTs. The substrates were prepared by sanding, washing in soap and water, and then ten minutes of 100 W Ar plasma treatment. Following preparation, the steel substrates were coated with 10 nm of aluminum (via thermal vapor deposition) before being placed inside a quartz tube positioned in a tube furnace. The main furnace was heated to 750°C while the preheater furnace was heated to 200°C under 500 sccm Ar and 100 sccm H_2 flow. Once the furnaces reached their proper temperatures, a floating catalyst method was used for growing the CNT arrays.[19] For VACNTs, ~66.7 mg mL^{-1} of ferrocene dissolved in xylene was used as the catalyst while for the VHCNTs the mixture was 66.7 mg mL^{-1} ferrocene, 83.2 mg mL^{-1} indium (III) isopropoxide, and 26.4 mg mL^{-1} tin (IV) isopropoxide in xylene. The isopropoxide salts are very sensitive to moisture and were handled inside of a glovebox which contained less than 10 ppm oxygen and moisture. For successful synthesis of HCNTs, the indium (III) isopropoxide should be off-white in color; if exposed to moisture it will appear orange in color and will not dissolve in xylene. Likewise, the tin (IV) isopropoxide should be white in color. These catalyst solutions were injected into the preheater furnace at 1.5 mL $hour^{-1}$ along with a flow of acetylene (40 sccm). The CVD run time ranged from 10-40 minutes to obtain arrays of different heights. All growth parameters were identical for VHCNTs and VACNTs, excepting the catalyst composition, in order to ensure the only difference between samples is the helicity and related properties.

2.2 Buckypaper fabrication

To fabricate the BPs, the CVD grown CNTs were removed from the steel substrates. Dispersions of HCNTs and MWCNTs were prepared such that they were 0.3 g L^{-1} while the surfactant (25 wt.% SDS and 75 wt.% SLS) was 3.3 g L^{-1}. Approximately 200 mL of each CNT dispersion was filtered through a Whatman Nylon filter and the resulting BP was peeled from the filter and dried prior to testing. Each BP was thoroughly rinsed with 600 mL of water, which then allowed a fair comparison of the lignin uptake by each type of CNT. BPs were also soaked in 5 g L^{-1} SLS solution in order to allow further polymer absorption.

2.3 Characterization

A Hitachi S-4800 scanning electron microscope was used to determine the heights of the arrays. Cyclic voltammetry (CV) and electrochemical impedance spectroscopy (EIS) were carried out on a Gamry 3000 potentiostat/galvanostat. Raman spectroscopy was performed using a Renishaw inVia micro-Raman system with an excitation wavelength of 785 nm. CVD grown CNTs were dispersed in methanol before being drop cast on glass for Raman spectroscopy; this approach to sample preparation allowed spectroscopic evaluation of the interior regions of the arrays instead of just their top surface. To conduct electrochemical analyses, a piece of the steel substrate covered with VHCNTs or VACNTs was used as the working electrodes in a home-built polytetrafluoroethylene 3-electrode test cell where 0.785 cm^2 of the active material was exposed to electrolyte. A platinum mesh was used as the counter electrode, and 1 M tetraethylammonium tetrafluoro-borate in acetonitrile was used as the electrolyte in a voltage range of -1.2 V to 1.2 V with respect to Ag/AgCl. Voltage scan rates of 3, 10, 30, and 100 mV/s were used for cyclic

voltammetry. For the BPs containing SLS, 1 M HNO_3 was used as the electrolyte to promote the redox reaction of the quinone group, with the voltage ranging from -0.2 V to 1 V with respect to Ag/AgCl. The BPs were cycled at 10 A g^{-1} for 10,000 cycles.

3. Results and discussion

When comparing the capacitances of VHCNTs or VACNTs grown on steel substrates, their values were not normalized by mass. To properly weigh the active material, the CNTs would need to be scraped from the circular electrodes used in the study, which would be difficult to accomplish, especially after the electrode's exposure to electrolyte salts. Therefore, the measured capacitance values were instead normalized by the array height and electrode area as reported in one of our previous publications.[15] SEM images showing CNT arrays of various heights can be seen in Fig. 1. Examples of typical CV plots for VACNTs and VHCNTs are shown in Figs. 2a and 2d, respectively. The measurements were made at 10, 30, and 100 mV s^{-1} scan rates, which show a purely capacitive response. The specific capacitance values of VHCNTs and VACNTs as a function of array height are shown in Figs. 2b and 2c, respectively. To determine the uncertainty in the height of each array, several sites on each substrate were analyzed via SEM to determine the average height of each array. The slopes of the linear fits to the data indicate that the capacitance of the VHCNTs exceeds that of the VACNTs, which is attributed to a combination of relatively higher surface area and defect density in VHCNTs. The defect density in a CNT is proportional to the intensity of the *D*-band in the Raman spectra which appears at ~1350 cm^{-1} (see Fig. 2e).[43] Clearly, the VHCNTs displayed a larger *D*-band compared to the VACNTs. A comparison of the *D*-band intensity as a function of plasma exposure for VACNTs and VHCNTs is displayed in supplementary figure S1. Upon Ar plasma treatment, VACNTs

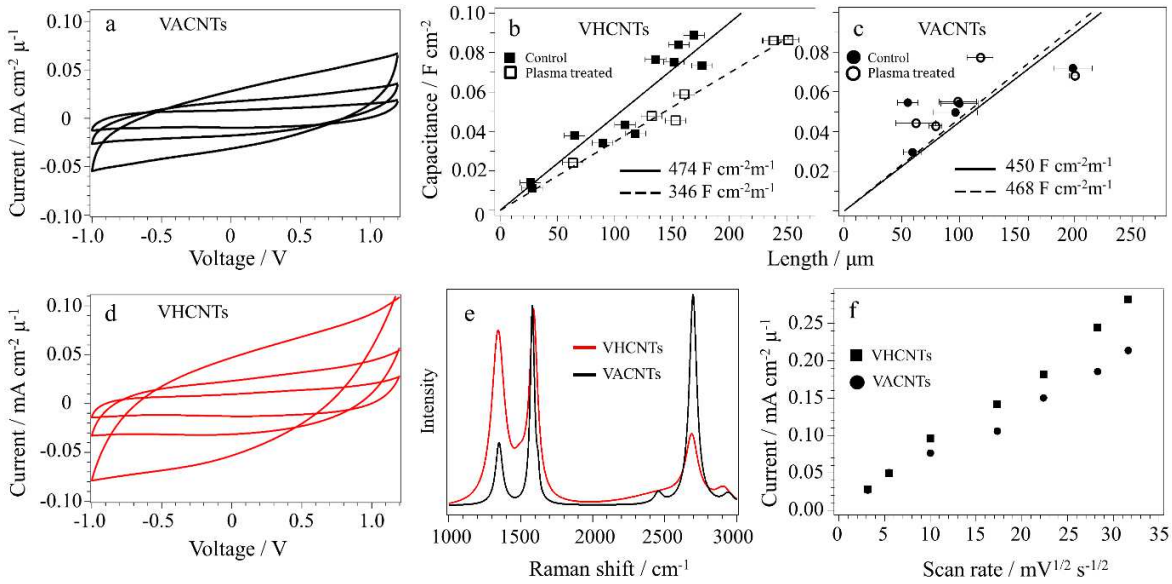

Figure 2. **a**) and **d**) Cyclic voltammograms taken at scan rates of 10, 30, and 100 mV s^{-1} for VACNTs and VHCNTs. Current values are normalized by electrode area (cm^2) and array height (μm^{-1}). **b**) and **c**) show capacitance versus array height for VHCNTs and VACNTs from CV data recorded at 100 mV s^{-1}. The data compare control samples to those exposed to 100 W Ar plasma for 10 minutes. The slopes of the trend lines are indicated below the data. The VHCNTs show a greater change in capacitance after plasma treatment than the VACNTs as shown by their respective trend lines. The VHCNT slope decreased by 28% while the VACNT slope increased by only 4%. **e**) The Raman spectra show VHCNTs to have a more prominent *D*-band at 1350 cm^{-1} compared to the VACNTs. **f**) Current vs. the square root of scan rate demonstrates linear trends indicating diffusion limited behavior.

displayed higher capacitance than the VHCNTs as evinced by their respective slopes in Figs. 2b and 2c. While the plasma treated VACNTs showed a small increase (~4%) in slope, the plasma treated VHCNTs showed a significant (~28%) decrease in slope, signaling an adverse influence of plasma treatment in the latter. Previous work has shown that Ar plasma can be used to enhance the capacitance of carbon nanostructures through the addition of extrinsic defects.[33,44] However, the plasma treatment of VHCNTs likely led to significant structural damage caused by Ar ion bombardment of the tube walls which already possessed a significant defect density. When comparing the surfaces of straight versus helical nanotubes, the surface energy of the latter is greater due to the torsional stresses on the hexagonal lattice of the tube

walls.[28] This higher surface energy would reduce the energy barrier required for creating defects on the surface during the plasma treatment, making HCNTs more susceptible to plasma exposure. A possible explanation for the small increase in VACNT performance following plasma treatment is that the plasma is only affecting the outer wall of the CNTs. Jorio *et al.* have studied similar effects by subjecting multiple layers of graphene to Ar ion bombardment.[45] They found that the ions only affected the outer layers of the graphene, which is analogous to the outer tube of a MWCNT. To determine how the arrays of linear and helically coiled morphologies affect ion diffusion, peak current versus the square root of scan rate are plotted in Fig. 2f. The trend remains linear after the initial low scan rates for VHCNTs and VACNTs, indicating diffusion limited charge/discharge behavior for each array. To summarize the first part of this study, the VHCNTs demonstrated superior capacitance to the VACNTs prior to plasma treatment, but suffered a greater loss in performance subsequent to plasma treatment.

The results for the second part of the experiment wherein BPs are compared will now be discussed. The structure of the as-grown HCNTs can be seen in Fig. 3a. The SEM image shows a cross section of a VHCNT array while the inset TEM image shows a closer view of the helical morphology. When preparing the BPs from HCNTs and MWCNTs, caution was taken to maintain the same mass ratios of surfactant to CNTs. The thermal gravimetric profile of each type of BP is shown in Fig. 3b. From the large difference in the loss of mass, it is evident that the HCNTs retained a higher amount of polymer than the MWCNTs during the fabrication of BPs. The drop in mass at 275°C is due to the loss of SDS surfactant while the loss starting after 300°C is attributed to the loss of SLS. In addition to the helical morphology that grants greater surface area for a given height, defects may also play a role in the superior adsorption of lignin by the HCNTs. The altered charge density localized to defects within the hexagonal lattice is known to

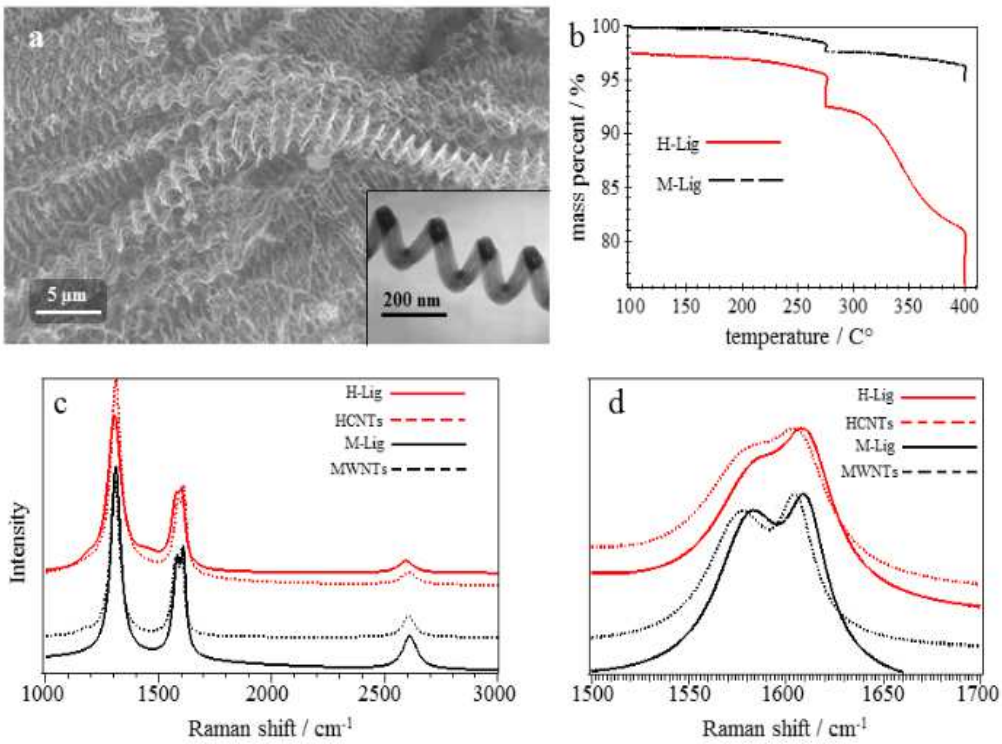

Figure 3. a) SEM image of HCNTs. The inset is a TEM image of a single helically coiled nanotube. b) TGA results of BPs made from HCNTs and MWCNTs. The lignin begins to burn off above 300°C and the HCNTs were found to hold more lignin than MWCNTs by mass percent. HCNTs also contained more SDS which is seen to burn off above 250°C. c) Raman spectra of pristine HCNTs and MWCNTs compared to lignin infused BPs, taken with 785 nm excitation. The *D′*-band located at ~1610 cm^{-1} is associated with defects and is typically much smaller than the *G*- and *D*-bands. However, under 785 nm excitation, both the *D* and *D′*-bands are much larger than those found using 532 nm excitation, possibly due to a resonance effect. d) Magnified view of the *G*-band. The *G*-band up-shifts after the lignin is adsorbed, indicating some degree of charge abstraction from the graphitic lattice.

have an effect on the binding energy of adsorbates.[46–48] This effect could also promote the adsorption of SLS onto HCNTs over MWCNTs due to the larger amount of defects present in HCNTs. Evidence for surfactant adsorption can be found in the Raman spectra of the prepared BPs. Raman spectra for each type of BP as well as the bare component CNTs are shown in Figs. 3c and 3d. The spectra were taken with 785 nm excitation and the *G*-band can be found at ~1580 cm^{-1}. When polymer is adsorbed to the surface of the CNTs, the vibrational modes of the hexagonal lattice are affected by the altered charge distribution, resulting in an upshift of the *G*-

band frequency by several wavenumbers (Fig. 3d). Specifically, the *G*-band for MWCNTs shifts from 1577 to 1584 cm^{-1} while for the HCNTs it shifts from 1580 to 1586 cm^{-1}. These shifts were found to remain consistent between multiple spectra. A previous report on this topic found that the polymer adsorption results in an upshift of the *G*-band frequency by ~10 cm^{-1}, which was attributed to van der Waals forces between the polymer and nanotube that increase the energy necessary for vibrations to occur.[40,49] It is also well known from the literature on graphite intercalation compounds that the *G*-band frequency will upshift in the presence of an electron accepting species.[50]

The electrochemical characteristics of each type of BP are displayed in Fig. 4. Figure 4a shows the redox reaction of lignin that occurs during cycling of the BPs. Nyquist plots of the impedance data for the BPs taken before and after 10,000 cycles at 10 A g^{-1} are displayed in Fig. 4b. The HCNT BPs possess a lower series resistance than the MWCNT BPs prior to and following cycling. We attribute the lower resistance to the coiled morphology of the HCNTs. Within the BP, the coils could create more points of contact between the tubes, thus leading to lower series resistance despite the presence of defects. After cycling, the high-frequency semi-circle becomes slightly depressed for the HCNTs, almost forming a second semi-circle. In a system that undergoes charge transfer between an electrolyte and substrate, the height of the high-frequency semi-circle is proportional to the charge transfer resistance. After cycling, the heights of semi-circle are approximately equal for HCNTs and MWCNTs, indicating similar charge transfer resistance. To determine which type of BP is more amenable for polymer adsorption, they were soaked in a 5 g L^{-1} SLS solution for 24 hours in order for them to adsorb additional amount of polymer. The soaking resulted in an increase of mass by 6% for the HCNTs and 2% for the MWCNTs as determined by microbalance measurements. These soaked samples displayed

similar EIS spectra to those found in Fig. 4b. In Fig. 4c, typical mass normalized CV curves for the BPs are displayed. Data is also displayed for a BP that was compressed at ~170 lbs in^{-2}. The redox reaction of the SLS associated with the quinone group is known to occur from ~0.55 to 0.6 V and is highly reversible. The larger peak was found to diminish after compression of the BPs,

indicating less charge transfer was able to occur for that case. Conversely, the smaller peak was unaffected by the compression indicating it may be due to a different source than the redox reaction of the quinone group. In this case, the diameter of the semi-circle in the Nyquist plot is also related to the diffusion resistance of ions migrating through the CNT/polymer system. This

was confirmed by conducting EIS on the compressed BP specimen, whose Nyquist plot is shown in the inset of Fig. 4c along with a control. By compressing the BP, the ability of molecules to diffuse through the system would be hindered while the series resistance would be decreased due to greater connectivity within the electrode. The reduced series resistance is shown by the Z′

intercept which is seen to decrease for the compressed sample. Concomitant with the reduced series resistance is an increase in the semi-circle diameter. It thus stands to reason that the increased diameter is related to the increased diffusion resistance. Past research found similar effects for the case of porous sulfur electrodes where compression led to an increase in semi-

circle diameter.[51] The capacitance of the HCNT BPs was found to be superior to that of the MWCNTs at all scan rates. This is reflected by the CV curves shown in Figs. 4d and 4e for MWCNT and HCNT BPs, respectively. The cycling rates ranged from 3 mV s^{-1} to 100 mV s^{-1}. For the 3 mV s^{-1} CV curves shown in Fig. 4c, the measured capacitances of the HCNT and

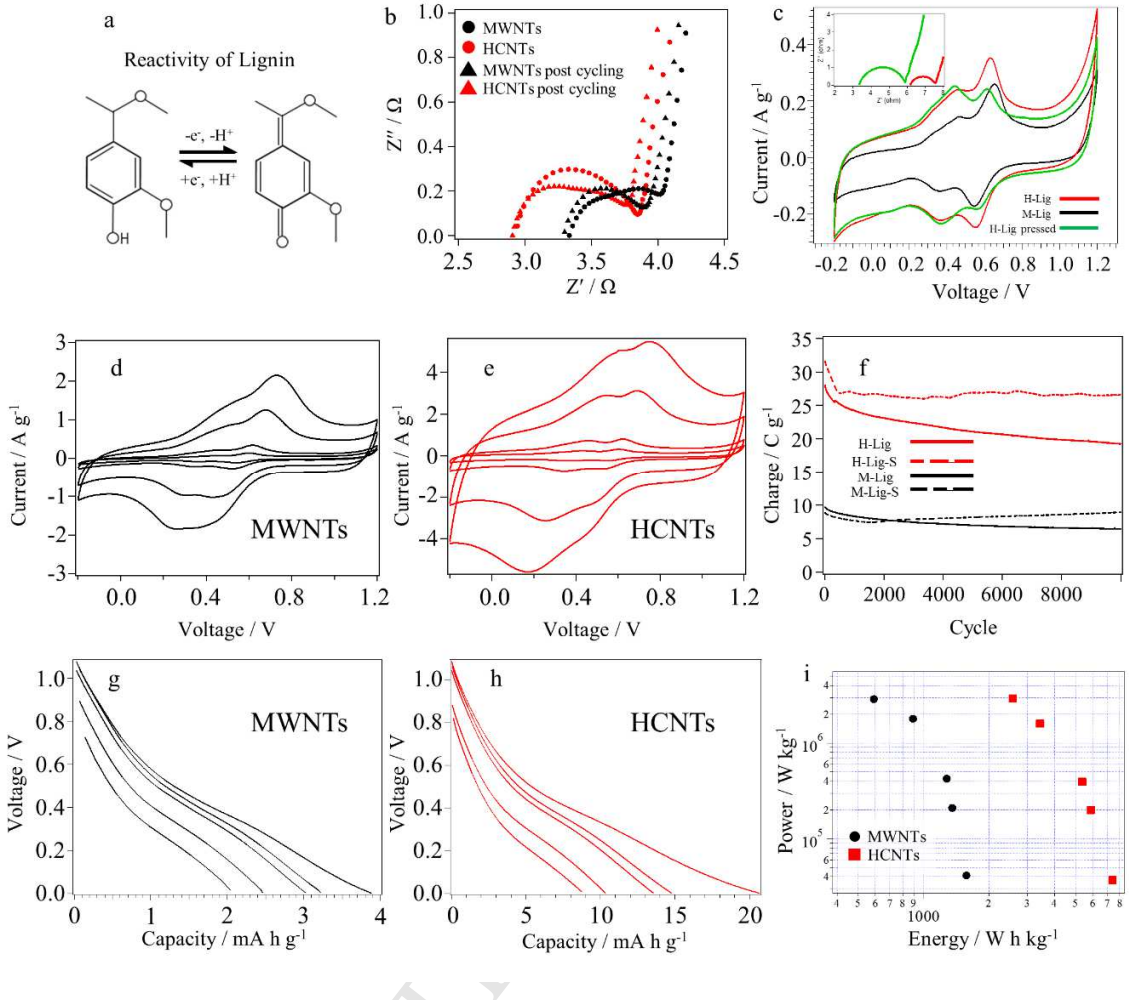

Figure 4. Electrochemical data for as-prepared and lignin solution soaked BPs. HCNT and MWCNT BPs are prefixed as H and M respectively, while the BPs soaked in lignin solution are suffixed with S. **a)** Redox reaction of SLS in acidic media. **b)** Nyquist plot for the BPs are compared before and after 10,000 cycles. **c)** Comparison of CV data taken at 3 mV s^{-1} for HCNT and MWCNT BPs. The capacitances measured from the curves of the HCNT and MWCNT BPs are 593 mF cm^{-2} (125.0 F g^{-1}) and 379 mF cm^{-2} (69.7 F g^{-1}), respectively. The inset shows Nyquist plots for an HCNT BP before (red) and after pressing (green). **d)** and **e)** CV curves of MWCNT and HCNT BPs respectively, taken at scan rates ranging from 3-100 mV s^{-1}. **f)** Comparison of the capacity of each type of BP after 10,000 cycles at 10 A g^{-1}. **g)** and **h)** Discharge curves for MWCNT and HCNT BPs respectively, ranging from 10 A g^{-1} to 0.1 A g^{-1}. **i)** Ragone plot showing power and energy densities.

MWCNT BPs are 593 mF cm^{-2} (125.0 F g^{-1}) and 379 mF cm^{-2} (69.7 F g^{-1}) respectively. It could be proposed that the coiled morphology of HCNTs lead to a structure of lower density that is better able to accommodate polymer and the flow of electrolyte, however we do not find that to be the case. This is because the measured mass densities of the HCNT and MWNT BPs are very

similar. If the HCNT BPs have more macroscopic void space, they would necessarily possess a lower density as well. Therefore, the large difference in specific capacitance cannot be explained in terms of the void space between nanotubes.

A potential problem with using redox polymers to enhance electrodes is that their structural integrity may be compromised after many cycles. To investigate the durability of the BP electrodes, they were cycled at a rate of 10 A g^{-1} for 10,000 cycles, and the results are shown in Fig. 4f. The increase in capacity is much greater for the HCNT BP compared to the smaller improvement for the MWCNT BP, which is attributed to the greater amount of adsorbed SLS in the former. Overall, the HCNT BPs demonstrate superior capacity to the MWCNT BPs. Traces showing the discharge capacity of the BPs are shown in Figs. 4g and 4h, where the discharge rates ranged from 10 A g^{-1} to 0.1 A g^{-1}. Energy and power densities calculated from the

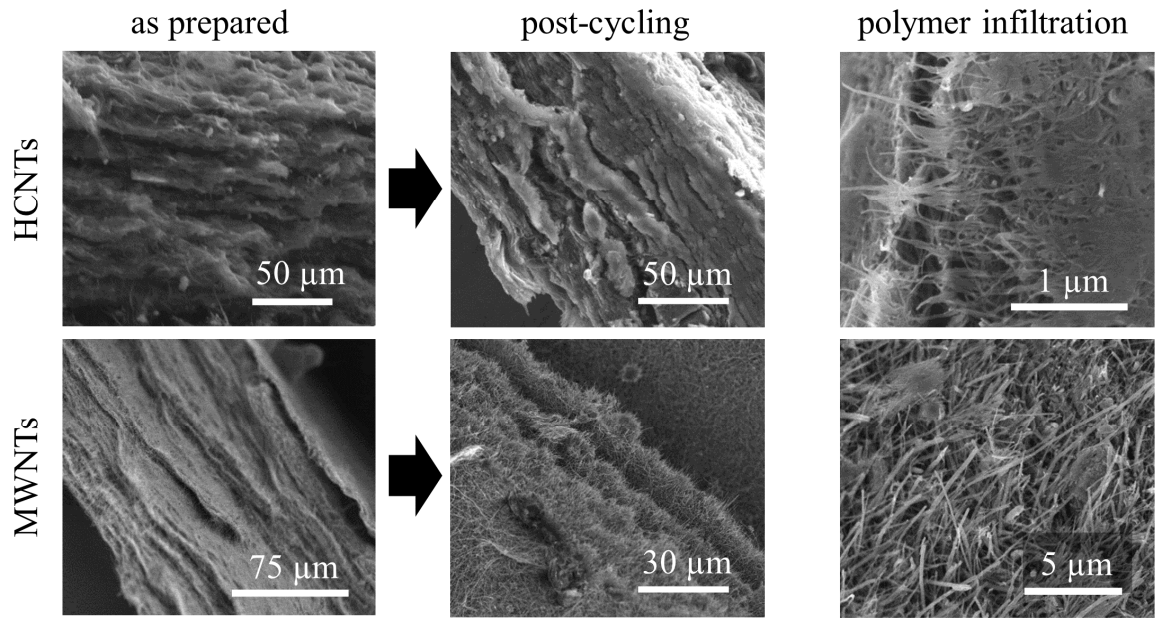

Figure 5. SEM images showing HCNTs (top) and MWCNTs (bottom) in as-prepared BPs, after 10,000 cycles at 10 A g^{-1}, and after soaking in SLS solution.

discharge curves are also displayed in the Ragone plot in Fig. 4i. Typically, power and energy densities are plotted for full cells, but it is included here since it is a direct comparison between electrodes where all things are equal besides morphology. While the HCNT BPs show greater energy density relative to MWCNT BPs, their power densities and capacity fades are similar. Structural changes in the BPs caused by soaking and cycling are revealed by the cross-sectional SEM images shown in Fig. 5. The center images correspond to BPs after constant current cycling, and no changes in the structure of the BPs are observed, consistent with their robust mechanical properties. The right images show the BPs after soaking in SLS, wherein the embedded polymer is evident.

4. Conclusions

We have grown HCNTs to evaluate their use as EDLC electrodes and compared their performance to electrodes made from VACNTs and MWCNT BPs. The capacitance of electrodes made from VHCNT and VACNT arrays display a linear dependence on array height and showed diffusion limited behavior below the maximum scan rate of 1 V s^{-1}. The VHCNT arrays exhibited greater capacitance than their VACNT analogs, however, upon Ar plasma treatment their performance deteriorated. The HCNT BPs showed a superior ability to adsorb polymer, and displayed capacitance values far exceeding those of the MWCNT BPs as well as the VHCNT and VACNT arrays. This study concludes that HCNTs are well suited for use as binder-free electrodes that can be augmented with electroactive polymers for improved performance.

Acknowledgements

The authors acknowledge the NSF Scalable Nanomanufacturing Award #CMMI-1246800 for funding this work, and thank Drs. Mark Roberts and Ramakrishna Podila for their insightful comments.

References:

[1] E. Frackowiak, K. Metenier, V. Bertagna, F. Beguin, Appl. Phys. Lett. 77 (2000) 2421.

[2] K.H. An, W.S. Kim, Y.S. Park, J.-M. Moon, D.J. Bae, S.C. Lim, Y.S. Lee, Y.H. Lee, Adv. Funct. Mater. 11 (2001) 387–392.

[3] E. Frackowiak, F. Béguin, Carbon N. Y. 40 (2002) 1775–1787.

[4] C. Masarapu, H.F. Zeng, K.H. Hung, B. Wei, ACS Nano 3 (2009) 2199–2206.

[5] G. Atthipalli, Y. Tang, A. Star, J.L. Gray, Thin Solid Films 520 (2011) 1651–1655.

[6] S. Dorfler, I. Felhosi, T. Marek, S. Thieme, H. Althues, L. Nyikos, S. Kaskel, J. Power Sources 227 (2013) 218–228.

[7] K.Y. Lee, Y.S. Lin, Y.M. Chen, Y.S. Huang, Phys. E-Low-Dimensional Syst. Nanostructures 42 (2010) 2799–2803.

[8] W. Lu, L.T. Qu, K. Henry, L.M. Dai, J. Power Sources 189 (2009) 1270–1277.

[9] M. Noked, S. Okashy, T. Zimrin, D. Aurbach, Carbon N. Y. 58 (2013) 134–138.

[10] C.L. Pint, N.W. Nicholas, S. Xu, Z.Z. Sun, J.M. Tour, H.K. Schmidt, R.G. Gordon, R.H. Hauge, Carbon N. Y. 49 (2011) 4890–4897.

[11] R. Reit, J. Nguyen, W.J. Ready, Electrochim. Acta 91 (2013) 96–100.

[12] R. Shah, X.F. Zhang, S. Talapatra, Nanotechnology 20 (2009) 395202.

[13] W. Lu, L. Qu, K. Henry, L. Dai, J. Power Sources 189 (2009) 1270–1277.

[14] R. Guzmán De Villoria, A.J. Hart, B.L. Wardle, ACS Nano 5 (2011) 4850–4857.

[15] M.R. Arcila-Velez, J. Zhu, A. Childress, M. Karakaya, R. Podila, A.M. Rao, M.E. Roberts, Nano Energy 8 (2014) 9–16.

[16] L. Oakes, T. Hanken, R. Carter, W. Yates, C.L. Pint, ACS Appl. Mater. Interfaces 7 (2015) 14201–14210.

[17] M. Karakaya, J. Zhu, A.J. Raghavendra, R. Podila, S.G. Parler, J.P. Kaplan, A.M. Rao, Appl. Phys. Lett. 105 (2014).

[18] X.B. Zhang, X.F. Zhang, D. Bernaerts, G. van Tendeloo, S. Amelinckx, J. van Landuyt, V. Ivanov, J.B. Nagy, P. Lambin, A.A. Lucas, Europhys. Lett. 27 (1994) 141–146.

[19] W. Wang, K.Q. Yang, J. Gaillard, P.R. Bandaru, A.M. Rao, Adv. Mater. 20 (2008) 179–182.

[20] C. Daraio, V.F. Nesterenko, S. Jin, W. Wang, A.M. Rao, J. Appl. Phys. 100 (2006) 064309.

[21] R. Thevamaran, M. Karakaya, E.R. Meshot, A. Fischer, R. Podila, A.M. Rao, C. Daraio, RSC Adv. 5 (2015) 29306–29311.

[22] X.-F. Li, K.-T. Lau, Y.-S. Yin, Compos. Sci. Technol. 68 (2008) 2876–2881.

[23] K. Lau, M. Lu, K. Liao, Compos. Part A Appl. Sci. Manuf. 37 (2006) 1837–1840.

[24] Q. Zeng, H. Tian, J. Jiang, X. Ji, D. Gao, C. Wang, RSC Adv. 7 (2017) 7375–7381.

[25] A. Leela Mohana Reddy, R.I. Jafri, N. Jha, S. Ramaprabhu, P.M. Ajayan, J. Mater. Chem. 21 (2011) 16103.

[26] R.B. Rakhi, W. Chen, H.N. Alshareef, J. Mater. Chem. 22 (2012) 5177.

[27] J. Zhu, A.S. Childress, M. Karakaya, S. Dandeliya, A. Srivastava, Y. Lin, A.M. Rao, R. Podila, Adv. Mater. 28 (2016) 7185–7192.

[28] S. Amelinckx, X.B. Zhang, D. Bernaerts, X.F. Zhang, V. Ivanov, J.B. Nagy, Science (80). 265 (1994) 635–639.

[29] P.R. Bandaru, C. Daraio, K. Yang, A.M. Rao, J. Appl. Phys. 101 (2007) 094307.

[30] J.H. Xia, X. Jiang, C.L. Jia, Appl. Phys. Lett. 95 (2009) 223110.

[31] V.D. Blank, B.A. Kulnitskiy, Carbon N. Y. 42 (2004) 3009–3011.

[32] J.A. Robinson, E.S. Snow, Ş.C. Bădescu, T.L. Reinecke, F.K. Perkins, Nano Lett. 6 (2006) 1747–1751.

[33] P.R. Bandaru, H. Yamada, R. Narayanan, M. Hoefer, Mater. Sci. Eng. R-Reports 96 (2015) 1–69.

[34] S. Ihara, S. Itoh, J. Kitakami, Phys. Rev. B 48 (1993) 5643–5647.

[35] B. Ashrafi, J. Guan, V. Mirjalili, P. Hubert, B. Simard, A. Johnston, Compos. Part A Appl. Sci. Manuf. 41 (2010) 1184–1191.

[36] J.-H. Han, H. Zhang, M.-J. Chen, G.-R. Wang, Z. Zhang, Compos. Sci. Technol. 103 (2014) 63–71.

[37] S. Wang, Z. Liang, G. Pham, Y.-B. Park, B. Wang, C. Zhang, L. Kramer, P. Funchess, Nanotechnology 18 (2007) 095708.

[38] A.M. Díez-Pascual, J. Guan, B. Simard, M.A. Gómez-Fatou, Compos. Part A Appl. Sci. Manuf. 43 (2012) 1007–1015.

[39] F.S. Chakar, A.J. Ragauskas, Ind. Crops Prod. 20 (2004) 131–141.

[40] G. Milczarek, in:, 9th IEE Conf. Nanotechnology, IEE NANO, 2009, p. 5394616.

[41] Y. Liu, L. Gao, J. Sun, J. Phys. Chem. C 111 (2007) 1223–1229.

[42] G. Milczarek, Langmuir 25 (2009) 10345–10353.

[43] F. Tuinstra, J.L. Koenig, J. Chem. Phys. 53 (1970) 1126–1130.

[44] M. Hoefer, P. Bandaru, J. Electrochem. Soc. 160 (2013) H360–H367.

[45] A. Jorio, M.M. Lucchese, F. Stavale, E.H.M. Ferreira, M.V.O. Moutinho, R.B. Capaz, C. a Achete, J. Phys. Condens. Matter 22 (2010) 334204.

[46] M.A. Hoefer, P.R. Bandaru, J. Appl. Phys. 108 (2010) 183108–34308.

[47] J.A. Nichols, H. Saito, C. Deck, P.R. Bandaru, J. Appl. Phys. 102 (2007) 064306.

[48] J.A. Robinson, E.S. Snow, Ş.C. Bădescu, T.L. Reinecke, F.K. Perkins, Nano Lett. 6 (2006) 1747–1751.

[49] V.A. Sinani, M.K. Gheith, A.A. Yaroslavov, A. Anna, K. Sun, A.A. Mamedov, J.P. Wicksted, N.A. Kotov, A.A. Rakhnyanskaya, Phys. Rev. Lett. (2005) 3463–3472.

[50] M.S. Dresselhaus, G. Dresselhaus, Adv. Phys. 51 (2002) 1–186.

[51] C. Barchasz, J.-C. Leprêtre, F. Alloin, S. Patoux, J. Power Sources 199 (2011) 322–330.